Adapalene-loaded poly(ε-caprolactone) microparticles: Physicochemical characterization and *in vitro* penetration by photoacoustic spectroscopy

Jessica Mendes Nadal [1]*, Guilherme dos Anjos Camargo[1], Andressa Novatski[2,3], William Roger Macenhan[2], Daniele Toniolo Dias[4], Fernanda Malaquias Barboza[1], Amanda Lyra[1], João Ricardo Roik[3], Josiane Padilha de Paula[1], Aloisi Somer[3], Paulo Vitor Farago[1,2]

1 Postgraduate Program in Pharmaceutical Sciences, Department of Pharmaceutical Sciences, State University of Ponta Grossa, Ponta Grossa, Paraná, Brazil, 2 Postgraduate Program in Health Sciences, State University of Ponta Grossa, Ponta Grossa, Paraná, Brazil, 3 Department of Physics, State University of Ponta Grossa, Ponta Grossa, Paraná, Brazil, 4 Academic Department of Physics, Federal University of Technology–Paraná, Ponta Grossa, Paraná, Brazil

* jessicabem@hotmail.com

OPEN ACCESS

Abstract

Adapalene (ADAP) is an important drug widely used in the topical treatment of acne. It is a third-generation retinoid and provides keratolytic, anti-inflammatory, and antiseborrhoic action. However, some topical adverse effects such as erythema, dryness, and scaling have been reported with its commercial formula. In this sense, the microencapsulation of this drug using polyesters can circumvent its topical side effects and can lead to the enhancement of drug delivery into sebaceous glands. The goal of this work was to obtain ADAP-loaded poly(ε-caprolactone) (PCL) microparticles prepared by a simple emulsion/solvent evaporation method. Formulations containing 10 and 20% of ADAP were successfully obtained and characterized by morphological, spectroscopic, and thermal studies. Microparticles presented encapsulation efficiency of ADAP above 98% and showed a smooth surface and spherical shape. Fourier transform infrared spectroscopy (FTIR) results presented no drug-polymer chemical bond, and a differential scanning calorimetry (DSC) technique showed a partial amorphization of the drug. ADAP permeation in the Strat-M membrane for transdermal diffusion testing was evaluated by photoacoustic spectroscopy (PAS) in the spectral region between 225 and 400 nm after 15 min and 3 h from the application of ADAP-loaded PCL formulations. PAS was successfully used for investigating the penetration of polymeric microparticles. In addition, microencapsulation decreased the *in vitro* transmembrane diffusion of ADAP.

Introduction

Adapalene (ADAP; $C_{28}H_{28}O_3$; MW: 412.52 g.mol^{-1}) or 6-[3-(1-adamantyl)-4-methoxyphenyl]-2-naphthalene-2-carboxylic acid (Fig 1) is a synthetic analog of retinol (vitamin A) used for the acne treatment [1,2]. The mechanism of action of ADAP is due to the selective interaction by specific retinoid intranuclear receptors (RARs), leading to the reduction of sebum production by sebaceous glands, reversing inflammatory lesions, follicular hyperkeratinization and the microcomedones formation [3–6]. The mechanism of action of ADAP also decreases the expression of the toll-like receptors 2 (TLR2) used by the *Propionibacterium acnes*, inhibiting the release of pro-inflammatory cytokines [4,5,7,8]. In addition, the modulation of the immune response occurs by altering the expression of CD1-d and IL10, causing an increase in the antimicrobial activity of the immune system [9–11]. During the early course of ADAP treatment, some local adverse events can be noticed such as: erythema, dryness, peeling, burning, and itching. To minimize these side effects, users need to decrease exposure to sunlight, avoid extreme temperatures, and use moisturizers [12].

In recent years, polymeric microparticles have aroused increasing interest as drug delivery systems. Many authors have reported that microparticles can be used to deliver active compounds into the skin in greater amounts than conventional topical formulations [13]. These microparticles are particularly interesting for the development of controlled release dosage forms. The microparticles also play an important role as drug carriers aiming to improve drug stability and minimize side effects [14]. Various methods are readily available for the microencapsulation of drugs, and one of the most commonly used is the simple emulsion/solvent evaporation [15].

Poly(ε-caprolactone) (PCL) is a linear synthetic polyester that is hydrophobic, biodegradable, and biocompatible. Because of the slow degradation and high stability, this polymer is suitable for the long term and controlled release of encapsulated drugs [16,17]. The PCL undergoes degradation by the hydrolysis of the ester linkages, generating ε-hydroxycaproic
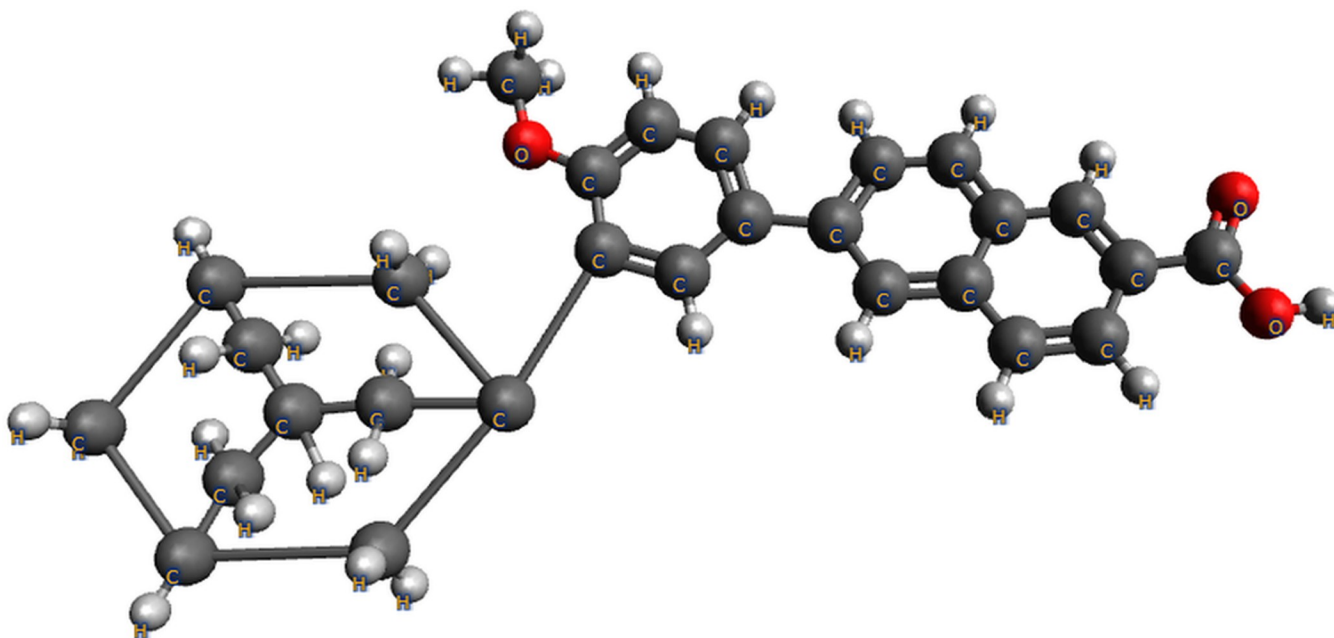

Fig 1. Chemical structure of adapalene (ADAP).

https://doi.org/10.1371/journal.pone.0213625.g001

acid. However, because of the high hydrophobicity, this reaction is slow and does not produce the acidic environment that occurs when using other polymers such as poly lactic acid (PLA) and poly lactic-*co*-glycolic acid (PLGA) [18]. Besides, the PCL mechanism of degradation includes bulk erosion in the aqueous medium and shows *in vitro* stability, facilitating its use in drug-controlled release systems [19].

One of the greatest current challenges for developing topical formulations is confirming if they permeate through different skin layers. In the case of pharmaceutical products, the active substance should reach the region of interest and maintains its properties even if the skin conditions undergo significant changes regarding moisture content, pH, and oxidative degradation [20]. Photoacoustic spectroscopy (PAS) [21] has been widely used as an alternative method to determine the percutaneous penetration of topically applied substances [20,22–24]. In particular, PAS is a non-destructive spectroscopic method that enables the carrying out of experiments that determine the drug penetration profile along skin thickness at depths up to about 200 μm. Thus, this method can be both used to study the penetration and drug distribution characteristics on the skin [20,22–24]. Although previous papers have widely established the application of PAS for predicting skin drug penetration, no previous report was devoted to investigating its use for evaluating the penetration and drug distribution in synthetic membranes.

Taking into account all these data, the hypothesis of this paper is that the microencapsulation into PCL microparticles may reduce ADAP transmembrane diffusion. At first, the ADAP-loaded microparticles were prepared by emulsion/solvent evaporation and characterized by morphological, spectroscopic, and thermal methods. Then, the encapsulation efficiency was determined by a previously validated UV method. The *in vitro* penetration was performed by photoacoustic spectroscopy using a synthetic membrane (Strat-M) to predict the diffusion through human skin. As far as we are aware, this is the first time that PAS is applied to investigate encapsulated drugs for topical application.

Materials and methods

Materials

Adapalene (ADAP, 99.13% pure, Fagron S.A., Rotterdam, Netherlands), poly(ε-caprolactone) (PCL) (M_w 10.000 g.mol^{-1}, Sigma-Aldrich, St. Louis, USA), poly(vinyl alcohol) (PVA) (*Mw* 72.000 g.mol^{-1}, 88.5 mol% of hydrolysis, Vetec, Rio de Janeiro, Brazil), and polysorbate 80 (Tween 80, Delaware, Porto Alegre, Brazil) were used as received. The other reagents and solvents were of analytical grade. Strat-M membrane was purchased from Merck Millipore (Billerica, MA, USA).

Preparation of adapalene-loaded PCL microparticles

The emulsion/solvent evaporation method was used to prepare the microparticles containing ADAP [16]. The composition of three formulations are presented in Table 1 and was dependent on the amount of ADAP (0, 10, and 20%). First, the ADAP and PCL were dissolved in dichloromethane, forming the organic phase that was added into the aqueous phase composed by poly (vinyl alcohol) (PVA) and polysorbate 80 under mechanical stirring (5000 rev.min^{-1}, RW 20 digital overhead paddle stirrer, IKA Works, Wilmington, NC, USA) for 5 min. The emulsion was kept under mechanical stirring (800 rev.min^{-1}, RW 20 digital overhead paddle stirrer, IKA Works, Wilmington, NC, USA) at room temperature for solvent evaporation. After 4 h, microparticles were separated by centrifugation (2000 rev.min^{-1}, 5 min, BE-4004 centrifuge, Bio Eng, São Paulo, Brazil) and washed three times with purified water to remove the adhered PVA on the surface of particles and the organic solvent. All samples were dried

Table 1. Composition of adapalene-loaded PCL microparticles.

Composition	Formulation		
	F0 (0%)	F10 (10%)	F20 (20%)
Aqueous phase			
Polysorbate 80 (g)	0.50	0.50	0.50
PVA (g)	4.00	4.00	4.00
Purified water (mL)	200.0	200.0	200.0
Organic phase			
Adapalene (ADAP) (g)	—	0.20	0.40
PCL (g)	2.00	1.80	1.60
Methylene chloride (mL)	40.0	40.0	40.0

under vacuum at 35 ± 1°C (TE-395 vacuum oven, Tecnal, Piracicaba, Brazil) for 6 h by sifting the powder through mesh 20 after drying. The obtained microparticles were stored in a desiccator under vacuum at room temperature. All formulations were obtained in triplicate. The negative control was the unloaded-microparticles (F0). A physical mixture (PM) containing ADAP and PCL at 1:1 ratio was also made.

Residual moisture

An infrared moisture analyzer (Top 160 Ray, Bel engineering, Monza, Italy) was used to evaluate the water content of pure ADAP, PCL, and microparticles. An amount of 0.050 g of each sample was placed on an aluminum plate and dried at 105°C until a constant weight was reached. The moisture content was obtained from the percentage corresponding to the mass loss. The tests were carried out in triplicate.

Characterization of adapalene-loaded PCL microparticles

Drug loading and encapsulation efficiency. In a volumetric flask, 10 mg of loaded and unloaded-microparticles was dissolved in acetone (20 mL) and stirred at 1000 rpm for 24 h. The volume was filled to 100 mL with purified water and filtered through a poly(vinylidene fluoride) membrane filter (Durapore membrane, 0.22 μm pore size, Millipore, Bedford, USA). After suitable dilution in ethanol, the drug concentration was spectrophotometrically determined at 321 nm (Hewlett Packard 8452A UV-Vis diode array spectrometer, Boeblingen, Germany) in triplicate. The UV method for ADAP quantification was previously validated in terms of linearity, precision, reproducibility, accuracy, and specificity. The concentration range varied from 4 to 12 $\mu g.mL^{-1}$. Linearity was 0.9998, and the detection limit was 0.35561 $\mu g.mL^{-1}$. The accuracy was 93.66% for 1.75 $\mu g.mL^{-1}$, 97.92% for 2.75 $\mu g.mL^{-1}$, and 97.34% for 3.75 $\mu g.mL^{-1}$. The repeatability presented a relative standard deviation (RSD) = 3.20, and the intermediate precision showed an RSD = 1.86. The encapsulation efficiency (EE) was then calculated using Eq 1:

$$EE = \left(\frac{mass\ of\ ADAP\ in\ microparticles}{theoretical\ mass\ of\ ADAP} \right) x100 \qquad (1)$$

Field emission gun scanning electron microscopy (FEG-SEM). The microparticles (F0, F10, and F20) were mounted on polished aluminum stubs, sputtered with gold (IC-50 Ion Coater, Shimadzu, Kyoto, Japan), and analyzed using a field emission gun scanning electron

microscope (FEG-SEM, TESCAN, model MIRA 3, Brno, Czech Republic) at an accelerating voltage of 15 kV with different magnifications.

Particle size. The particle size distribution was estimated from the measurement of 200 particles, assuming a spherical shape, observed in an arbitrarily chosen area of enlarged micrographs using the measurement toolbox for MATLAB (Mathworks Inc., Natick, MA, USA). The span was calculated using Eq 2:

$$span = \frac{d_{(v,90)} - d_{(v,10)}}{d_{(v,50)}}$$ (2)

where $d_{(v,10)}$, $d_{(v,50)}$, and $d_{(v,90)}$ are the particle diameters determined, respectively, at the 10th, 50th, and 90th percentiles of the undersized particle distribution curve.

Fourier-transformed infrared (FTIR) spectroscopy. The Fourier-transformed infrared (FTIR) spectra of ADAP, PCL, polymeric microparticles, and PM were recorded on a Shimadzu IR Prestige-21 spectrophotometer. (Kyoto, Japan). 4 mg of each sample were mixed with 100 mg of KBr, and the pellets were prepared under a pressure gauge of 80 kN. The spectra were obtained from 4000 to 400 cm^{-1}, with 32 scans and a resolution of 4 cm^{-1} in absorbance mode.

Differential scanning calorimetry (DSC). DSC measurements were performed using a DSC-60 (Shimadzu, Kyoto, Japan). The samples of ADAP, PCL, PM, and microparticles were packed in an Al_2O_3 crucible. The heating rate was 10 K.min^{-1} and under dynamic N_2 atmosphere (flow rate: 50 mL.min^{-1}) with a temperature range from 20 to 500°C. The DSC cell was calibrated with indium (m.p. = 429.6 K; ΔHfusion = 28.54 J. g^{-1}) and zinc (m.p. = 692.6 K).

Characterization of Strat-M membrane

Photoacoustic analysis. The photoacoustic spectroscopy (PAS) can evaluate the permeation profile by varying the modulation frequency and analyzing the absorption spectra by the photoacoustic (PA) signal. The permeation profile is measured when the drug characteristic band is observed [20,23,24]. The sample depth contributing to the PA signal is estimated using the thermal diffusion length $\mu_s = (\alpha/\pi f)^{1/2}$, in which α is the sample thermal diffusivity and f is the light modulation frequency [20,23,24].

The open photoacoustic cell (OPC) technique was applied as described in [25,26] to obtain the thermal diffusivity of the membrane. The PA signal in a function of f for a monochromatic been was recorded and analyzed by Eq 3:

$$PA = \frac{1}{f}\frac{C_1\alpha_s^{1/2}}{\sinh(l_s\sigma_s)} + \frac{1}{f^{3/2}}\frac{C_2\alpha_s^{3/2}}{\sinh(\sigma_s l_s)}\left[\cosh(\sigma_s l_s) - \frac{\sigma_s l_s}{2}\sinh(\sigma_s l_s) - 1\right]$$ (3)

where $\sigma_s = (1 + i)\sqrt{\pi f/\alpha_s}$ is the complex diffusion coefficient and C_1 and C_2 are adjust constants [25,26]. Five measurements were performed at different points of the membrane.

Field emission gun scanning electron microscopy (FEG-SEM) for the membranes. To correlate the thermal diffusivity data and the depth of penetration, the cross section of Strat M was evaluated using the same FEG-SEM applied for microparticles, with 200X of magnification.

Photoacoustic spectroscopy of Strat-M membrane. The photoacoustic spectroscopy (PAS) homemade setup was used for evaluating the Strat-M membrane, and the schematic apparatus is presented in Fig 2. This apparatus consisted of a Xenon lamp with 800 W (6269, Oriel Instruments, Newport Corporation, Franklin, MA, USA) as the light source, monochromator (CornerstoneTM 260 1/4m, Oriel Instruments), mechanical chopper (SR540, Stanford
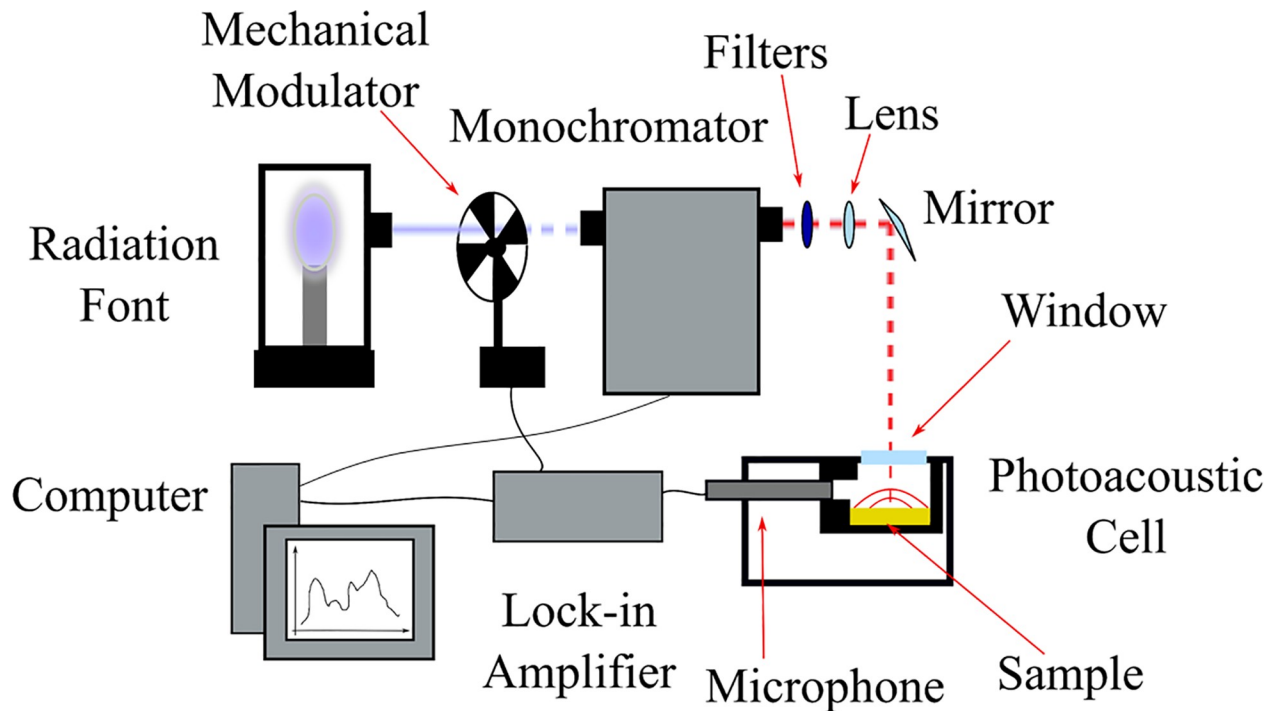
Fig 2. Schematic setup of photoacoustic spectroscopy. The radiation font, the mechanical modulator, monochromator, filters, lens, microphone as the detector, and a personal computer for data acquisition.

https://doi.org/10.1371/journal.pone.0213625.g002

Research Systems, Sunnyvale, CA, USA), lock-in amplifier (SR830, Stanford Research Systems), and microphone (4953, Brüel and Kjaer Instruments, Santo Amaro, Brazil) coupled to a sealed photoacoustic cell for signal detection. Higher order diffractions were eliminated by bandpass filters. The spectral range for UV-Vis was between 225 and 400 nm because of the ADAP and loaded microparticles characteristics absorptions. The chopper was tuned to different frequencies to modulate the light that impinges the sample. The data acquisition was performed by a personal computer. To correct the source emission intensity in each wavelength, all spectra were normalized with respect to a carbon black sample signal.

In vitro permeation studies

The measurements of the permeation profile were performed using a Strat-M membrane that was lighted on the opposite side of the surface applied with the formulations using the PAS setup. The membrane samples were analyzed after 15 min and 3 h from the application of ADAP, PM, F10, and F20 formulations. To choose the modulation frequencies, two factors were considered: values that could provide a depth profile through the membrane and values that were not multiples of the electrical power grid (60 Hz), which can cause noise effects. Besides, from the OPC technique and FEG-SEM results it was possible to determinate that frequencies 5, 23, 51, and 203 Hz provided satisfactory depth scan through the membrane.

Gaussian curve fitting. The absorption spectrum can be determined by a Gaussian curve based on wavelength (λ) because absorption intensity is directly related to the square of dynamic momentum. Thus, the amount of absorbing material is associated with peak area, which can be measured by a multi-peak Gaussian fit. Therefore, Gaussian curves were used in this work to measure peak areas and not to interpret the related absorbing substances. Since the peak positions from the spectra of both formulations and membrane used in the analysis

Table 2. Water content[1], adapalene-loaded[1], encapsulation efficiency (EE)[2], particle size[1] and span for PCL microparticles.

Microparticles	Water content (%)	Adapalene-loaded (mg.g^{-1})	EE (%)	Mean diameter (μm)	*Span*
F0	3.06 ± 0.09	—	—	8 ± 4	0.89
F10	2.7 ± 0.1	100 ± 2	100.44	8 ± 3	1.25
F20	2.91 ± 0.04	199 ± 2	99.37	7 ± 3	1.02

[1]means (*n* = 3) ± standard deviation

[2]means (*n* = 3)

were comparative, we assumed that this mathematical procedure is suitable to quantify the spectra and interpret the permeation of ADAP-loaded microparticles in the synthetic membrane. A detailed report about these analyses is in the supplementary material.

Results and discussion

Water content and encapsulation efficiency

After drying, all the obtained formulations showed powder aspect and white color similar to PCL. This result showed that the emulsion/solvent evaporation method successfully achieved the ADAP-loaded PCL microparticles preparation. Water contents of 5.70 ± 0.10% and 1.30 ± 0.10% were obtained for pure ADAP and PCL, respectively. In contrast, microparticles showed only residual moisture values, as presented in Table 2.

These data demonstrate that the performed vacuum drying was able to remove the water used during microencapsulation. The residual water content in a powder influences its physical stability and controls the magnitude of capillary forces that hold particles in aggregate [27]. Considering the obtained results, it is possible to expect that the water content has a low interference on the physical stability of PCL microparticles.

Table 2 also summarized the drug content and EE for ADAP-loaded microparticles. High percentages of drug entrapment were obtained for PCL microparticles by simple emulsion/solvent evaporation. Also, all formulations showed suitable EE values higher than 99%. These values are mainly based on the poor aqueous solubility (4.01 μg.L^{-1}) of ADAP [28], leading to an increase in the drug loaded into microparticles.

Field emission gun scanning electron microscopy (FEG-SEM). FEG-SEM analysis showed that PCL microparticles do not contain pores on their surface. All samples presented a spherical and almost spherical shape and had a smooth and slightly flaky surface (Fig 3). Previous studies that obtained PCL microparticles by the simple emulsion/solvent evaporation technique observed the same morphological data [16,29,30]. Unloaded-microparticles had similar morphology and size to formulations F10 and F20.

Particle size. The mean particle sizes obtained for unloaded and ADAP-loaded PCL microparticles are presented in Table 2. All formulations were micrometer-sized. Formulations F0, F10, and F20 showed mean diameters of about 8 *μ*m. Earlier studies demonstrated that microparticles with a diameter ranging from 3 to 10 *μ*m can be randomly distributed into the hair follicles and *stratum corneum* [13,31]. Hence, the particle size obtained from ADAP-loaded PCL microparticles are suitable to site-specific drug delivery to the hair follicles. In addition, PCL microparticles (F0, F10, and F20) revealed span values lower than 2 [32], representing a narrow polydispersity around the mean. Thus, these microparticles had a unimodal behavior, as requested for this topical pharmaceutical form.
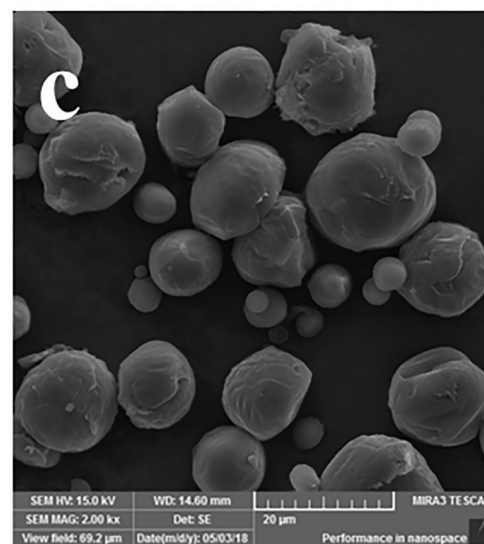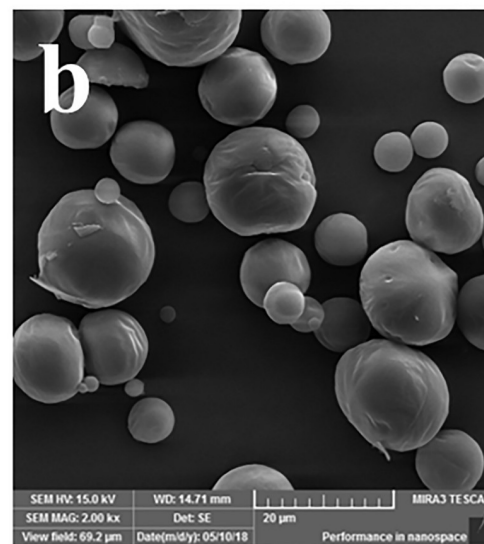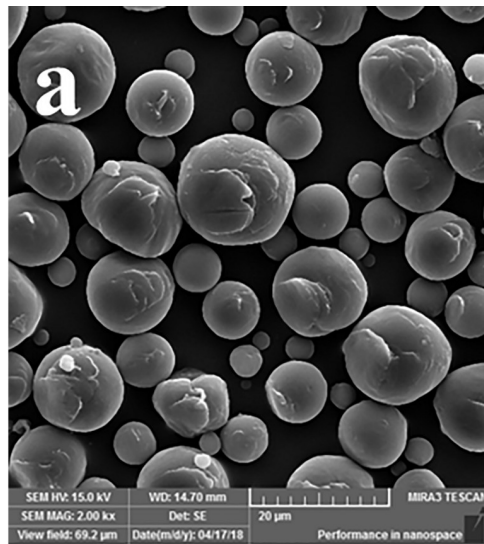
Fig 3. Scanning electron micrographs of PCL microparticles: F0 (a), F10 (b) and F20 (c). Magnifications of 2000X presenting a spherical shape and smooth, slightly flaky surface.

Fourier-transformed infrared (FTIR) spectroscopy

FTIR spectroscopy was performed in order to explore whether the microencapsulation resulted in any chemical change by comparing differences in band assignments among raw materials and formulations. FTIR results of ADAP, PCL, PM, and PCL microparticles are presented in Fig 4. The ADAP infrared spectra revealed absorption bands at 2903 cm^{-1} (C–H stretch in aldehyde and ketone), 2849 cm^{-1} (carboxylic O–H stretch), 1688 cm^{-1} (C = O stretch), 1477 cm^{-1} (C = C stretch), 1300 cm^{-1} (–C–O stretch), 1140 cm^{-1}, and 810 cm^{-1} (aromatic stretch, out-of-plane bend) [27,33–35]. The PCL infrared spectrum presented typical bands at 2945 cm^{-1} (asym CH$_2$ stretch), 2866 cm^{-1} (sym CH$_2$ stretch), 1730 cm^{-1} (ester C = O stretch), and 1060–1150 cm^{-1} (asym C–O–C stretch) [36]. Considering their FTIR spectra, ADAP-loaded PCL microparticles and PM presented band assignments at the same wavenumber ranges as those of the PCL and ADAP results. The broadening peaks at 2866, 2901, and 2949 cm^{-1} for F20 formulation is attributed to O–H and CH$_2$ stretch vibrations from the drug and polymer, respectively. Consequently, the microencapsulation process does not induce chemical interactions between the drug and PCL and ADAP, ensuring the drug's expected anti-acne effect.

Differential scanning calorimetry (DSC)

The DSC results for pure ADAP, PCL, PM, and PCL microparticles are presented in Fig 5. ADAP showed an endothermic event at 326˚C related to the melting point in accordance with the literature [35]. PCL presented a melting temperature of 67˚C and a decomposition temperature of 416˚C (endothermic events), confirmed by previously reported data [36]. The endothermic event at 305˚C can be related to a first event degradation process due to the rupture of the polyester chains of PCL [37]. PM sample presented endothermic peaks at 68 and 416˚C attributed to melting point and decomposition of PCL, respectively. The peak at 310˚C is because of the melting point of ADAP. For unloaded and ADAP-loaded microparticles (F0, F10, and F20), we noticed the endothermic events at 61 and 414˚C that attributed to the melting and decomposition points of PCL. There are no events attributed to ADAP in these samples, indicating a complete drug amorphization. The lack of events is probably because of the loosening crystal forces of ADAP molecularly dispersed within PCL that can favor an increase of drug water solubility [38].

Strat-M membrane characterization

To obtain the depth profile through the membrane, it is necessary to determinate the thermal diffusion length (μ) that measures the thickness of the parcel of the sample that most contributes to PA signal generation. In the present permeation study, this category of thermal thickness is proportional to the thermal diffusivity of the Strat-M membrane which is unknown. In this context, Fig 6 shows a frequency scan of the PA signal obtained by the OPC technique for the Strat-M membrane with a thickness of 310 μm. A good agreement of experimental data and theoretical fit by Eq (2) was observed, and the mean thermal diffusivity measured was α_s = $(7.0\pm0.5)\times10^{-7}$ m^2.s^{-1}. This value has the same order of magnitude as those of human skin (~ 1.36 x 10^{-7} m^2.s^{-1}) and of synthetic polymeric materials (~1.1 x10^{-7} m^2.s^{-1}, which is typical for low-density polyethylene and polyethylene terephthalate) [36]. As far as we are aware, this is the first report determining the thermal diffusivity for the Strat-M membrane. Therefore,
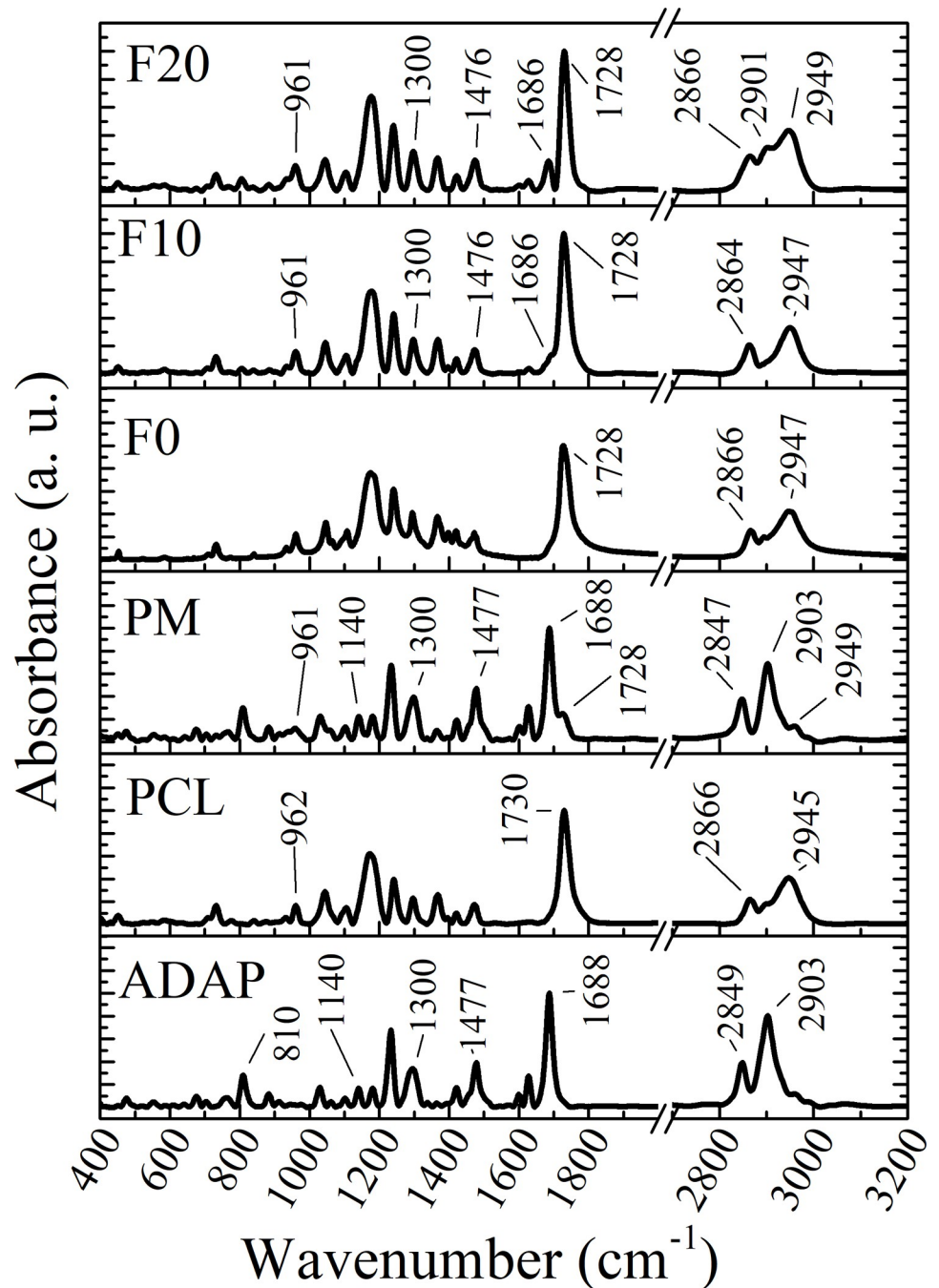
Fig 4. FTIR results of ADAP, PCL, PM, and PCL microparticles (F0, F10, and F20). PM presented bands at 1140, 1300, 1477, 1688, 2847, and 2903 cm^{-1} that are related to ADAP; bands at 961, 1728 and 2949 cm^{-1} that are attributed to PCL. The F10 and F20 do not present any shifts on these bands. In this case, the encapsulation process does not induce chemical interaction between the drug and PCL.

modulation frequencies at 5, 23, 51, and 203 Hz will provide a depth scan ($\mu_{membrane}$) of 210, 100, 67, and 34 μm, respectively.

The spectra obtained by PAS for the Strat-M membrane at 5, 23, 51, and 203 Hz are presented in Fig 7A. We can notice a redshift by increasing the modulation frequency, and the
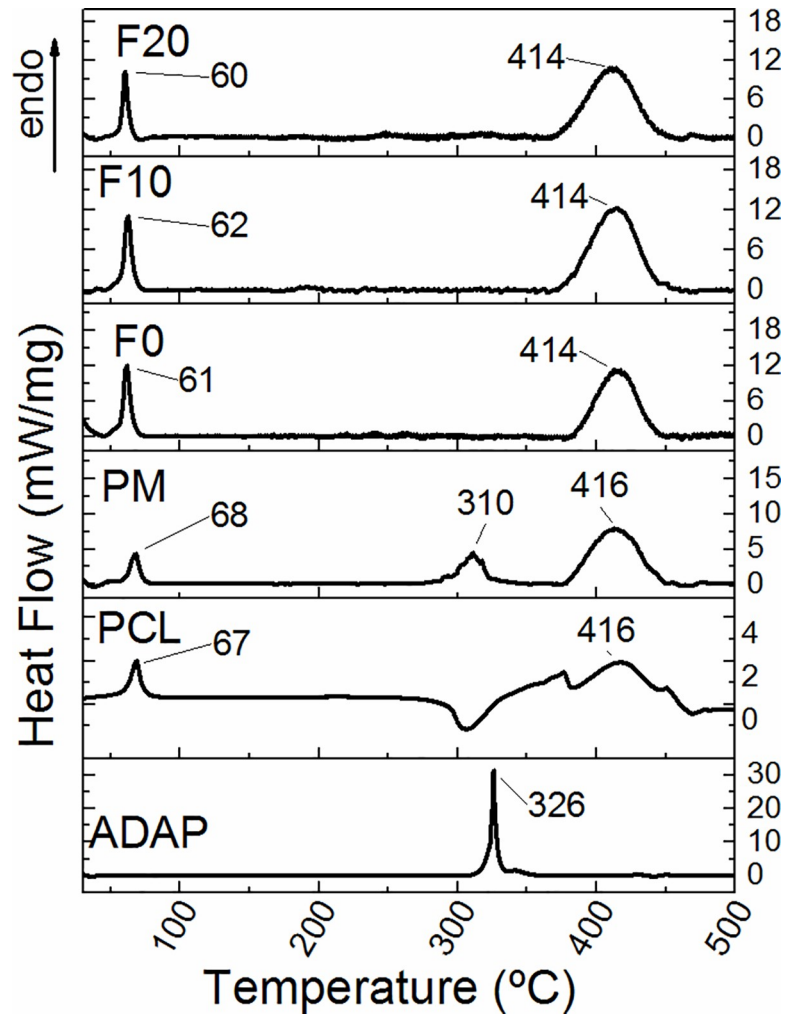
Fig 5. DSC curves of ADAP, PCL, PM, and PCL microparticles (F0, F10, and F20). The formulations F10 and F20 do not present the melting point of ADAP at 326˚C, showing a complete drug amorphization.

shift becomes more prominent from 5 to 23 Hz (210 to 100 μm in depth). This shift is attributed to the difference between the polymeric layers of membrane, which is explored in the following paragraphs. FEG-SEM results (Fig 7) confirmed the difference between the layers. For better visualization, the depth lengths ($\mu_{membrane}$) are marked with arrows.

According to the literature [32,34], the Strat-M membrane is composed of two layers of poly(ether sulfone) with a very tightly packed surface that provides some opposition to drug permeation. Above these layers, a layer of polyolefin is placed with a more open net that is therefore more permeable. From these polymeric layers, a porous structure with blends of synthetic lipids is provided that furnishes a gradient of pore size that changes diffusivity. The difference in pore sizes is shown in Fig 7B.

To further explore the PAS results for the Strat-M, a fit using two Gaussian curves for all spectra was performed that had a peak centered at 280 nm and a broad band centered at 300 nm. The band at 280 nm remains at the same position for the spectra for all frequencies (see supplementary material). In contrast, the broad band maintained the half-width of 100 nm, but the center shifted from 300 nm at 5 Hz to 350 nm at 203 Hz. These bands are related to the
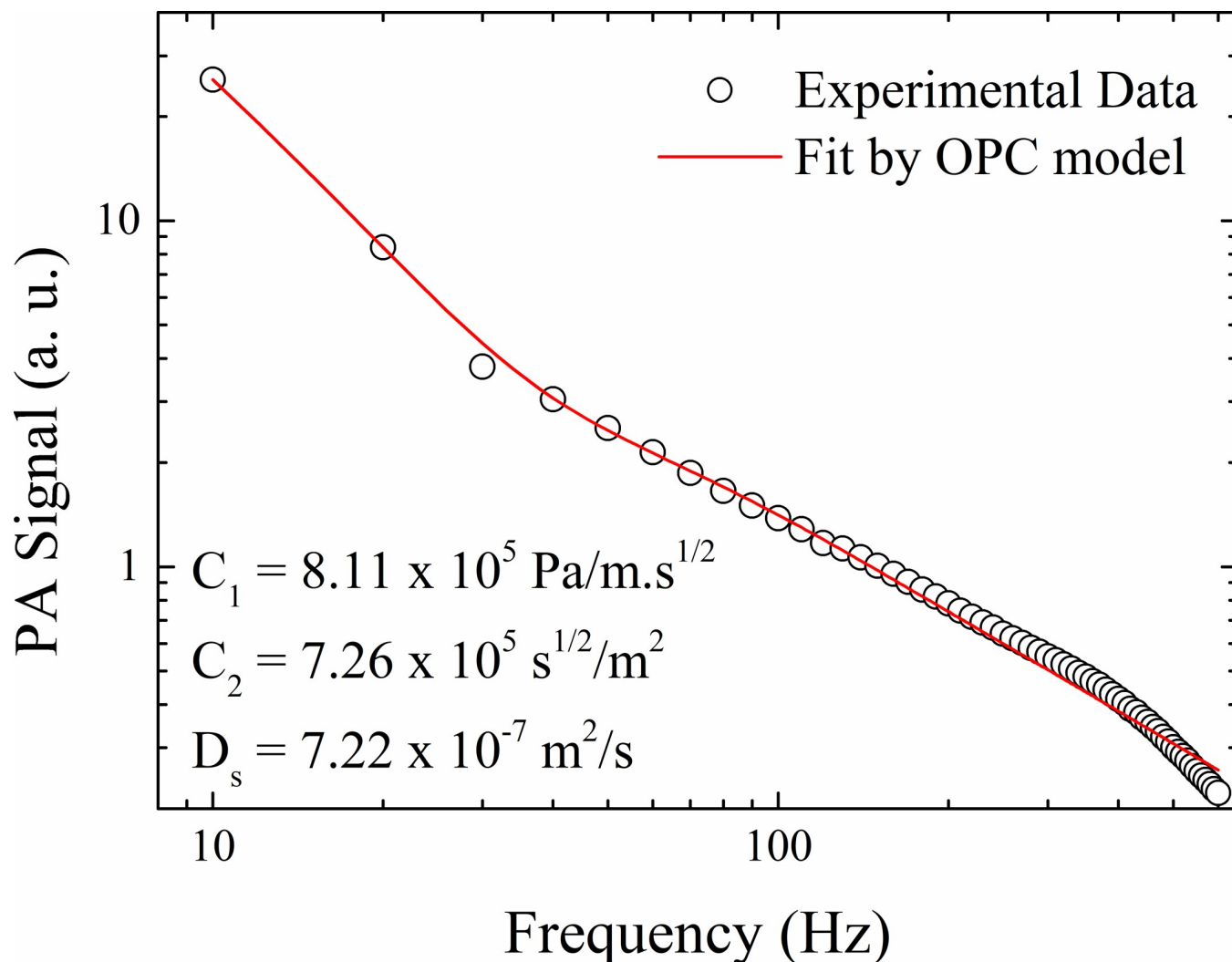
Fig 6. Experimental data of frequency scan by OPC technique for the Strat-M membrane with a thickness of 310±10 μm. The solid line represents the best data fit by Eq (2).

$\pi \rightarrow \pi^*$ transition associated with the π electrons in the benzene rings and mostly a function of the intra-chain interaction [39,40]. The shift from 300 to 350 nm means the polymeric chains become less entangled, so for a modulation frequency of 5 Hz (210 μm), the generated photoacoustic signal was from the poly(ether sulfone). The other frequencies generated photoacoustic signals in the polyolefin layer. Summarizing, the spectroscopic behavior of membrane with different values of modulation frequencies is associated with the change in the membrane layer. This is an important step in understanding the structure of Strat-M membrane, which is necessary to understanding *in vitro* permeation studies.

In vitro permeation study

To determine the permeation of ADAP in Strat-M membrane, the absorption spectra of ADAP and formulations of ADAP-loaded PCL microparticles must first be obtained. Fig 8A shows the ADAP spectra obtained by PAS spectroscopy, in which three Gaussian curves centered at 272, 336, and 369 nm were used to obtain the total spectrum (see supplementary
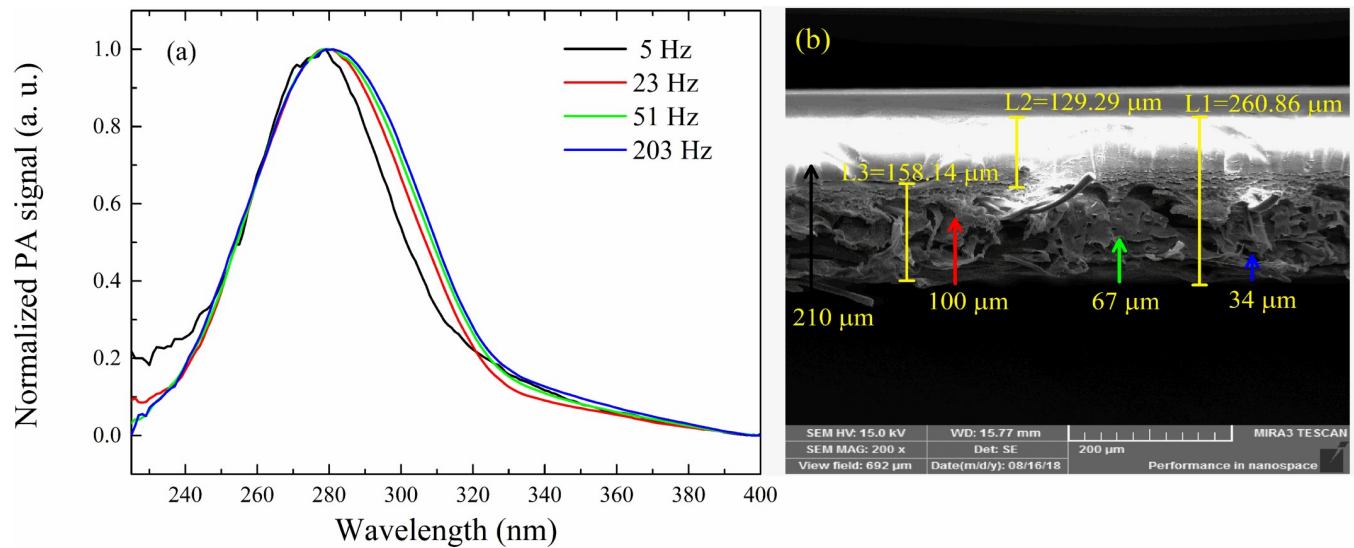
Fig 7. (a) PAS result for the Strat-M membrane. We can notice a redshift with decreasing depth, indicating the difference of the polymeric layers from the membrane. (b) FEG-SEM image of the membrane with 200x of magnification. The arrows illustrate the thermal diffusion length ($\mu_{membrane}$) obtained for frequencies of 5, 23, 51, and 203 Hz, and the colors are the same as the respective spectrum from (a).

material) in accordance with the literature [41,42]. F10 and F20 formulations (Fig 8B and 8C) were fitted with the Gaussian curves using the same position and width parameters of the ADAP. We can notice a decrease in intensity of the bands centered at 336 and 369 nm. These bands are attributed to transitions between π-electron energy levels of the aromatic rings of ADAP ligand. This decrease is an indication that the drug molecules are enclosed in polymeric microparticles.

To detect the formulation after application on the synthetic membrane, the redshift of the broad band of Strat-M with increasing modulation frequency was considered. The total spectrum was constructed by simulating each contribution using the absorption bands widths and centers of the formulations (Fig 8) and untreated membrane (Fig 7). The intensities of Strat-M bands were maintained constant. Because PCL did not show a PA signal, we considered the ADAP Gaussians curves for the PM sample.

Fig 9 presents the results for excitation in the internal side of the membrane for a 203 Hz modulation frequency (33 μm depth) after 15 min of applying the formulations. The Gaussian fitting was performed based on five peaks centered at 280 and 300–350 nm from the membrane and 272, 336, and 369 from the formulations. The *in vitro* permeation of each formulation can be evaluated by summing the areas under the Gaussian curves related to ADAP for each thermal diffusion length. For this, the Gaussian fit was made for all the obtained spectra at each frequency (see supplementary material for details). The same procedure was performed for the membranes submitted to the formulations after 3 h of application. The results permeation as a function of the thermal diffusion length is presented in Fig 10. The figure shows that the peak centered at 272 nm (related to ADAP) shifted to approximately 250 nm. This shift can be considered for the adjust because it recurrs for the same frequencies and is in accordance with the literature [41,42].

Fig 10A reveals that after 15 min, the drug absorption was constant of the surface at 100 μm and was the most intense for 210 μm. Thus, the highest drug concentration remains at approximately 210 μm for all formulations. However, after 3 h, (Fig 10B) the behavior is different for all formulations. For the ADAP sample, the most intense absorption occurred close to the
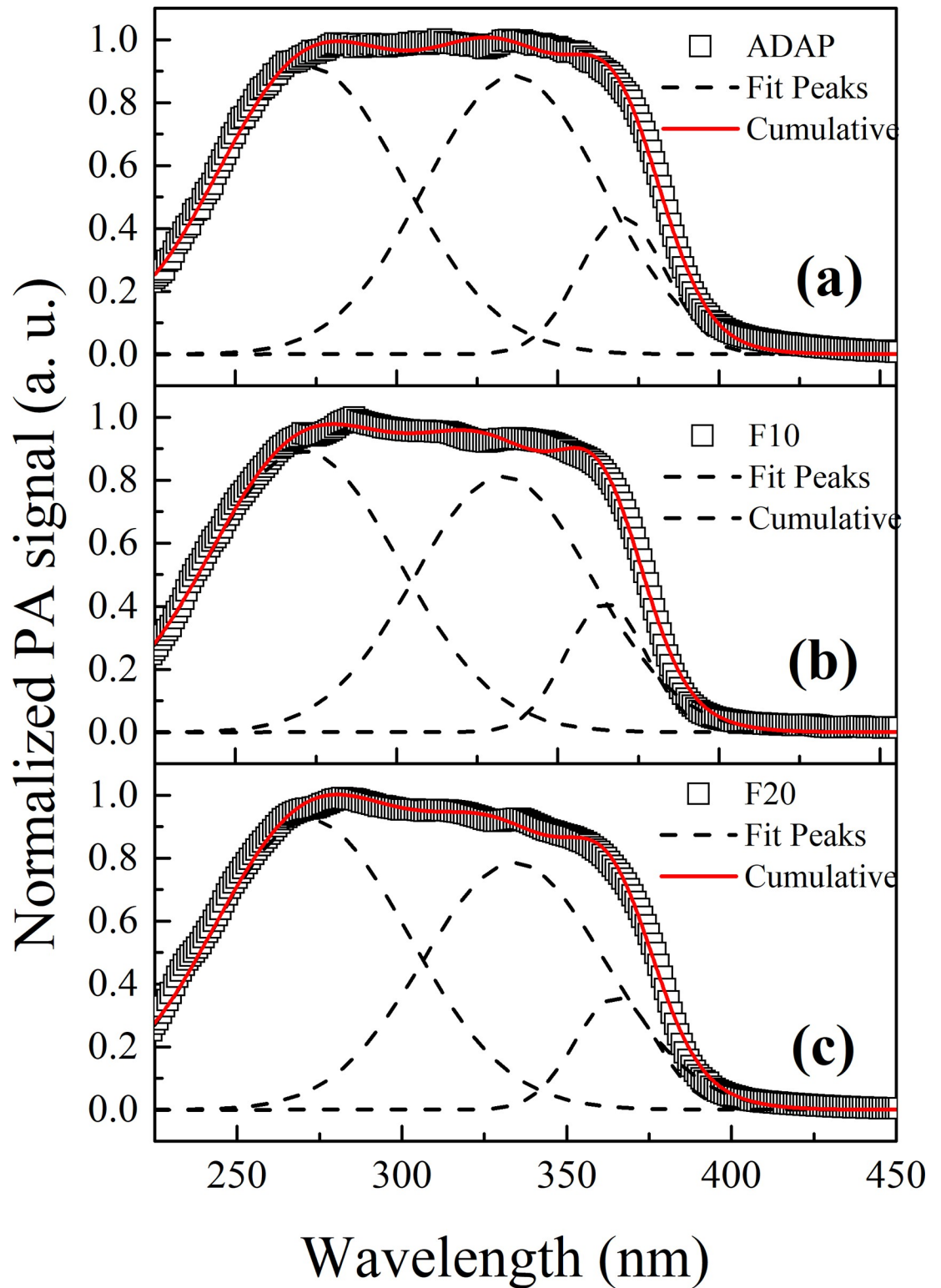
Fig 8. Photoacoustic spectra of formulations. ADAP and ADAP-loaded PCL microparticles. The Gaussian curves are centered at 272, 336, and 369 nm. The bands at 336 and 369 nm decrease in intensity for F10 and F20, indicating the enclosure of the drug molecules into polymeric microparticles.
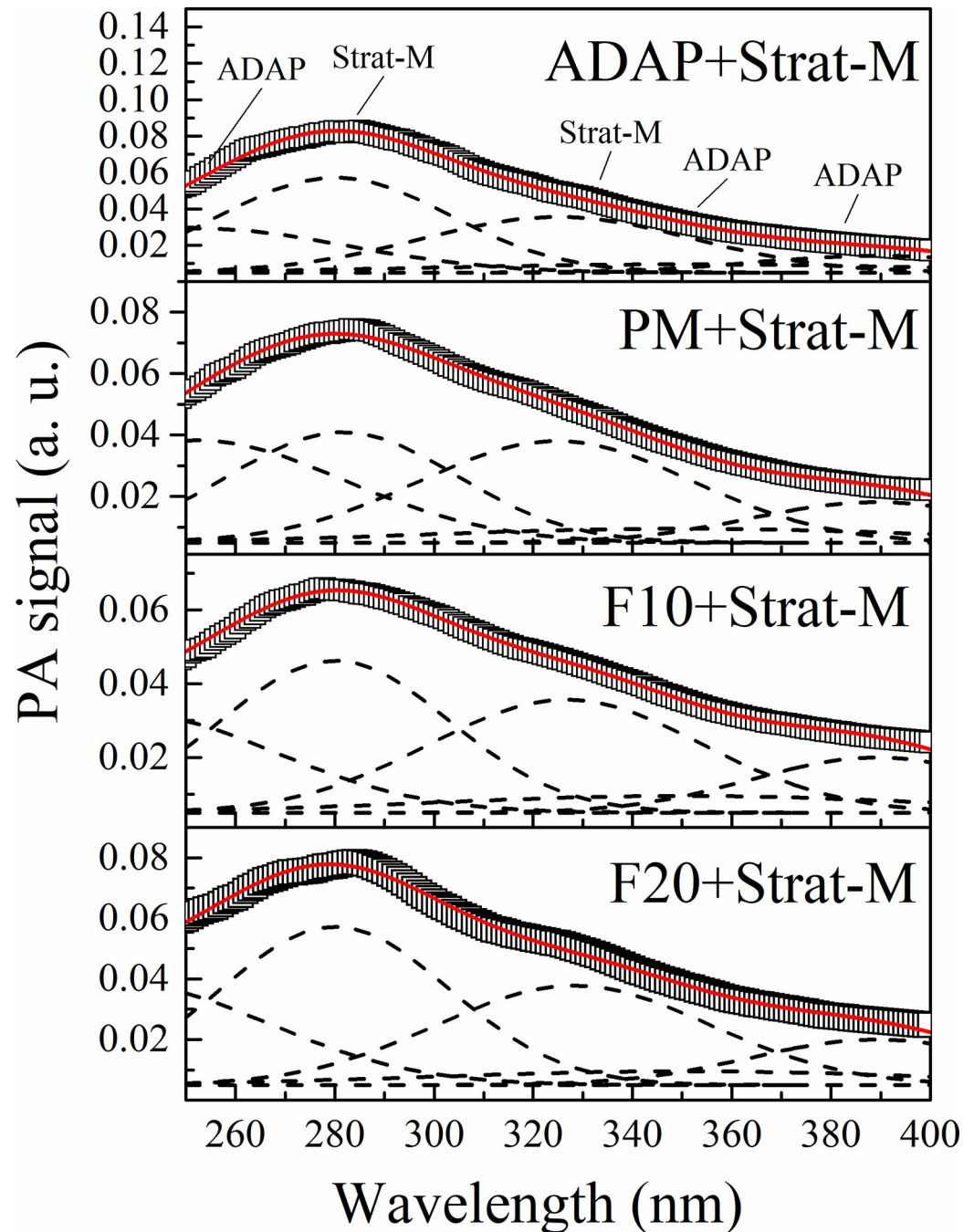
https://doi.org/10.1371/journal.pone.0213625.g008

Fig 9. Photoacoustic spectra for the membranes after 15 min of application formulations (Formulation+Strat-M).
Excitation in the internal side of the membrane with a 203 Hz modulation frequency (33 µm depth). The figure indicates the position of the peaks attributed to ADAP (250–269, 336 and 370–380 nm) and Strat-M (280, 300–350 nm).

https://doi.org/10.1371/journal.pone.0213625.g009

surface, indicating that the drug was detected and permeated through all layers of the membrane until 33 µm. Furthermore, most of the drug permeated through the membrane because the drug's contribution to larger diffusion lengths is lower. For the PM sample, the drug band absorption remains constant from 100 to 33 µm, indicating that the drug is spread through the membrane. The intensity of absorption of F10 presents a large increase of 210 to 100 µm and is
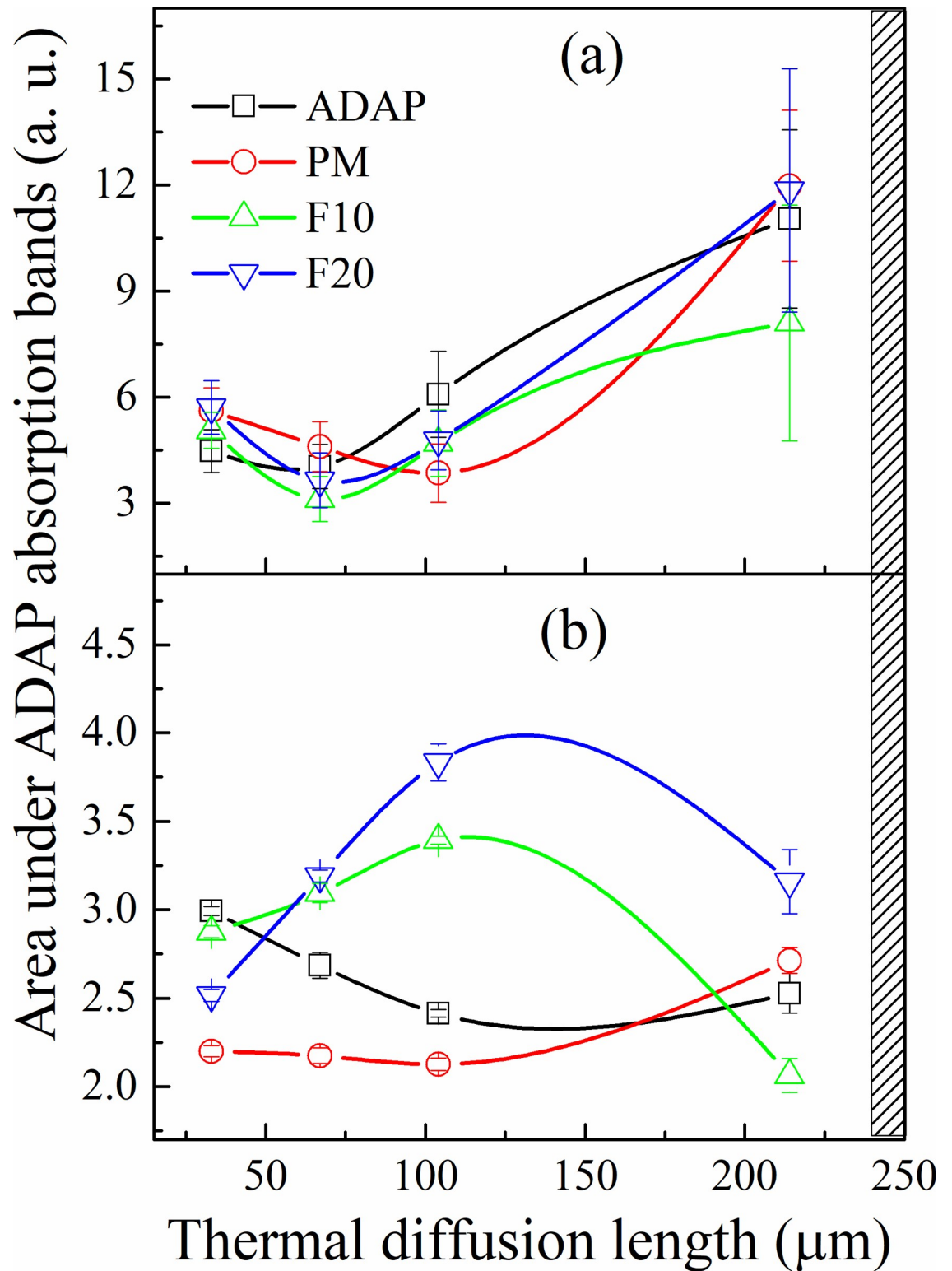
Fig 10. Evolution of ADAP permeation in the membrane as a function of thermal diffusion length after 15 min (a) and 3 h (b) of application obtained by the sum of the areas under the Gaussian curves related to ADAP (250–269, 336, and 370–380 nm). The hatched marks are approximately the positions where the formulations were applied. After 15 min, the highest drug concentration remains at approximately 210 μm for all formulations. After 3h, for ADAP and PM formulation, the drug permeates through all layers of the membrane until 33 μm. The F10 and F20 concentrate ADAP in 100 μm of penetration depth.

slightly attenuated at 33 μm. Thus, a considerable amount of the drug permeates at 100 μm. The behavior of F20 is similar of the F10. However, the increase of intensity from 210 to 100 μm is much smaller, and the attenuation at the surface is most intense. This result shows that the encapsulation process controls the permeation of ADAP, demonstrating that ADAP-loaded microparticles are suitable for the pharmacological application.

According to the literature, it is possible to compare Strat-M membrane layers to human skin layers [39]. The poly(ether sulfone) compact surface is equivalent to the *stratum corneum* and the polyolefin region is equivalent to the dermis in the skin reaching the follicular pathway. Analyzing the Strat-M membrane from the internal side, our results provided an intensification of this equivalence. The equivalent *stratum corneum* region has a 210 μm penetration depth, and the *dermis* region has a 100 μm penetration depth.

Considering this equivalence, pure ADAP and PM spread through all layers from the *stratum corneum* to the *dermis*. In contrast, formulations F10 and F20 were concentrated in the 100 μm region, and the amount of the drug that diffused to the region equivalent to the subcutaneous tissue of the human skin is much lower when compared to the amount that diffused through for pure ADAP.

Summarizing these remarks, the ADAP-loaded PCL microparticles provide a suitable system for topical treatment. The encapsulation process considerably reduces the permeation of the drug into different membrane layers, indicating that the ADAP will target the *dermis* in future *in vivo* studies, which is the targeting region for acne treatment.

Conclusion

ADAP-loaded PCL microparticles were effectively prepared by a simple emulsion/solvent evaporation method. Micrometer-sized formulations with high drug-loading efficiencies were obtained. No changes in FTIR assignments were recorded after the microencapsulation procedure. In addition, the photoacoustic spectroscopy showed that the microencapsulation decreased the *in vitro* transmembrane diffusion of ADAP, highlighting the particular characteristic of this technique to estimate the permeation of drugs through synthetic membranes. In summary, these formulations can be used in further innovative skin products intended for treating acne.

Supporting information

S1 Fig. Scheme of the raw data treatment obtained by photoacoustic spectroscopy for the membrane Strat M using 23 Hz as the modulation frequency.
(DOCX)

S2 Fig. Scheme of the raw data treatment obtained by photoacoustic spectroscopy from ADAP and formulations of ADAP-loaded PCL microparticles.
(DOCX)

S3 Fig. Scheme of the raw data treatment obtained by photoacoustic spectroscopy from the synthetic membrane treated with ADAP and formulations of ADAP-loaded PCL microparticles after 15 min and 3h of treatment.
(DOCX)

S1 Table. Adjust parameters obtained from Gaussian fitting performed on photoacoustic spectroscopy spectra for the membrane Strat M.
(DOCX)

S2 Table. Adjust parameters obtained from Gaussian fitting performed on photoacoustic spectroscopy spectra for ADAP and formulations.
(DOCX)

S3 Table. Adjust parameters obtained from Gaussian fitting for synthetic membrane after 15 min and 3h of treatment of ADAP and formulations.
(DOCX)

Author Contributions

Conceptualization: Jessica Mendes Nadal.

Formal analysis: Andressa Novatski, Josiane Padilha de Paula.

Investigation: Andressa Novatski, Daniele Toniolo Dias, João Ricardo Roik, Aloisi Somer.

Methodology: Jessica Mendes Nadal, Guilherme dos Anjos Camargo, William Roger Macenhan, Daniele Toniolo Dias, Amanda Lyra, João Ricardo Roik, Josiane Padilha de Paula, Aloisi Somer.

Project administration: Aloisi Somer, Paulo Vitor Farago.

Supervision: Jessica Mendes Nadal, Andressa Novatski, Daniele Toniolo Dias, Paulo Vitor Farago.

Validation: Guilherme dos Anjos Camargo, Fernanda Malaquias Barboza, Amanda Lyra.

Writing – original draft: Jessica Mendes Nadal, Guilherme dos Anjos Camargo, Andressa Novatski, Daniele Toniolo Dias, Aloisi Somer.

Writing – review & editing: Jessica Mendes Nadal, Andressa Novatski, Daniele Toniolo Dias, Paulo Vitor Farago.

References

1. Bernard BA. Adapalene, a New Chemical Entity with Retinoid Activity. Skin Pharmacol Physiol [Internet]. 1993; 6(suppl 1)(Suppl. 1):61–9. Available from: https://www.karger.com/DOI/10.1159/000211165

2. Osman-Ponchet H, Sevin K, Gaborit A, Wagner N, Poncet M. Fixed-Combination Gels of Adapalene and Benzoyl Peroxide Provide Optimal Percutaneous Absorption Compared to Monad Formulations of These Compounds: Results from Two In Vitro Studies. Dermatol Ther (Heidelb) [Internet]. 2017; 7 (1):123–31. Available from: https://doi.org/10.1007/s13555-016-0159-9

3. Shroot B, Michel S, Galderma FC, Antipolis S. Pharmacology and chemistry of adapalene. J Am Acad Dermatol. 1997; 36(6):S96–103.

4. Brogden RN, Goa KL. Adapalene. Drugs. 1997; 53(3):511–9. https://doi.org/10.2165/00003495-199753030-00010 PMID: 9074847

5. Michel S, Jomard A, Demarchez M. Pharmacology of adapalene. Br J Dermatol. 1998; 139:3–7.

6. Waugh J, Noble S, Scott LJ. Adapalene. Drugs. 2004; 64(13):1465–78. https://doi.org/10.2165/00003495-200464130-00005 PMID: 15212561

7. Thiboutot D. Regulation of human sebaceous glands. J Invest Dermatol. 2004; 123(1):1. https://doi.org/10.1111/j.1523-1747.2004.t01-2-.x PMID: 15191536

8. Jugeau S, Tenaud I, Knol AC, Jarrousse V, Quereux G, Khammari A, et al. Induction of toll-like receptors by Propionibacterium acnes. Br J Dermatol. 2005; 153(6):1105–13. https://doi.org/10.1111/j.1365-2133.2005.06933.x PMID: 16307644

9. Tenaud I, Khammari A, Dreno B. In vitro modulation of TLR-2, CD1d and IL-10 by adapalene on normal human skin and acne inflammatory lesions. Exp Dermatol. 2007; 16(6):500–6. https://doi.org/10.1111/j.1600-0625.2007.00552.x PMID: 17518990

10. Bikowski JB. Mechanisms of the comedolytic and anti-inflammatory properties of topical retinoids. J drugs dermatology JDD. 2005; 4(1):41–7.

11. Lheure C, Grange PA, Ollagnier G, Morand P, Désiré N, Sayon S, et al. TLR-2 recognizes Propionibacterium acnes CAMP factor 1 from highly inflammatory strains. PLoS One. 2016; 11(11):e0167237. https://doi.org/10.1371/journal.pone.0167237 PMID: 27902761

12. Phillips TJ. An update on the safety and efficacy of topical retinoids. Cutis. 2005; 75(2 Suppl):14–22. PMID: 15773539

13. Rolland A, Wagner N, Chatelus A, Shroot B, Schaefer H. Site-specific drug delivery to pilosebaceous structures using polymeric microspheres. Pharm Res. 1993; 10(12):1738–44. PMID: 8302759

14. Ahmad M, Madni A, Usman M, Munir A, Akhtar N, Khan HMS. Pharmaceutical micro encapsulation technology for development of controlled release drug delivery systems. World Acad Sci Eng Technol. 2011; 75(1):384–7.

15. Li M, Rouaud O, Poncelet D. Microencapsulation by solvent evaporation: State of the art for process engineering approaches. Int J Pharm. 2008; 363(1–2):26–39. https://doi.org/10.1016/j.ijpharm.2008.07.018 PMID: 18706988

16. Justus B, Nadal JM, Almeida MA, Janzen MES, Budel JM, Esmerino LA, et al. Benzoyl Peroxide-Loaded PCL Microparticles: Physicochemical Characterization and In Vitro Antibacterial and Permeation Studies. Lat Am J Pharm. 2015; 34(9):1710–7.

17. Kumari A, Yadav SK, Yadav SC. Biodegradable polymeric nanoparticles based drug delivery systems. Colloids Surfaces B Biointerfaces. 2010; 75(1):1–18. https://doi.org/10.1016/j.colsurfb.2009.09.001 PMID: 19782542

18. Chen DR, Bei JZ, Wang SG. Polycaprolactone microparticles and their biodegradation. Polym Degrad Stab. 2000; 67(3):455–9.

19. Behera AK, Barik BB, Joshi S. Poly-ε-caprolactone based microspheres and nanospheres: a review. FS J Pharm Res. 2012; 1(2):38–45.

20. Mota JP, Carvalho JLC, Carvalho SS, Barja PR. Photoacoustic technique applied to skin research: characterization of tissue, topically applied products and transdermal drug delivery. In: Acoustic Waves-From Microdevices to Helioseismology. InTech; 2011.

21. Rosencwaig A. Photoacoustics and photoacoustic spectroscopy. Wiley; 1980.

22. Ames FQ, Sato F, de Castro L V, de Arruda LLM, da Rocha BA, Cuman RKN, et al. Evidence of anti-inflammatory effect and percutaneous penetration of a topically applied fish oil preparation: a photoacoustic spectroscopy study. J Biomed Opt. 2017; 22(5):55003. https://doi.org/10.1117/1.JBO.22.5.055003 PMID: 28492854

23. De Melo JO, Pedrochi F, Baesso ML, Hernandes L, Truiti MCT, Baroni S, et al. Evidence of deep percutaneous penetration associated with anti-inflammatory activity of topically applied Helicteres gardneriana extract: a photoacoustic spectroscopy study. Pharm Res. 2011; 28(2):331–6. https://doi.org/10.1007/s11095-010-0279-3 PMID: 20859659

24. Rocha JCB, Pedrochi F, Hernandes L, de Mello JCP, Baesso ML. Ex vivo evaluation of the percutaneous penetration of proanthocyanidin extracts from Guazuma ulmifolia using photoacoustic spectroscopy. Anal Chim Acta. 2007; 587(1):132–6. https://doi.org/10.1016/j.aca.2007.01.002 PMID: 17386764

25. Somer A, Camilotti F, Costa GF, Bonardi C, Novatski A, Andrade AVC, et al. The thermoelastic bending and thermal diffusion processes influence on photoacoustic signal generation using open photoacoustic cell technique. J Appl Phys. 2013;114(6).

26. Somer A, Camilotti F, Costa GF, Jurelo AR, Assmann A, De Souza GB, et al. Effects of thermal oxidation on the effective thermal diffusivity of titanium alloys. J Phys D Appl Phys. 2014; 47(38).

27. Goyani M, Akbari B, Chaudhari S, Jivawala R. Formulation and evaluation of topical emulgel of antiacne agent. Int J Adv Res Rev. 2018; 3(7):52–68.

28. Karadzovska D, Riviere JE. Assessing vehicle effects on skin absorption using artificial membrane assays. Eur J Pharm Sci. 2013; 50(5):569–76. https://doi.org/10.1016/j.ejps.2013.02.020 PMID: 23474357

29. Gomes MLS, da Silva Nascimento N, Borsato DM, Pretes AP, Nadal JM, Novatski A, et al. Long-lasting anti-platelet activity of cilostazol from poly (ε-caprolactone)-poly (ethylene glycol) blend nanocapsules. Mater Sci Eng C. 2019; 94:694–702.

30. Mendes JBE, Riekes MK, de Oliveira VM, Michel MD, Stulzer HK, Khalil NM, et al. PHBV/PCL microparticles for controlled release of resveratrol: physicochemical characterization, antioxidant potential, and effect on hemolysis of human erythrocytes. Sci World J. 2012;2012.

31. Toll R, Jacobi U, Richter H, Lademann J, Schaefer H, Blume-Peytavi U. Penetration profile of microspheres in follicular targeting of terminal hair follicles. J Invest Dermatol. 2004; 123(1):168–76. https://doi.org/10.1111/j.0022-202X.2004.22717.x PMID: 15191557

32. Chew NYK, Chan H-K. Effect of powder polydispersity on aerosol generation. J Pharm Pharm Sci. 2002; 5(2):162–8. PMID: 12207868

33. Jain S, Kale DP, Swami R, Katiyar SS. Codelivery of benzoyl peroxide & adapalene using modified liposomal gel for improved acne therapy. Nanomedicine. 2018; 13(12):1481–93. https://doi.org/10.2217/nnm-2018-0002 PMID: 29972675

34. Bhalekar M, Upadhaya P, Madgulkar A. Formulation and evaluation of Adapalene-loaded nanoparticulates for epidermal localization. Drug Deliv Transl Res. 2015; 5(6):585–95. https://doi.org/10.1007/s13346-015-0261-z PMID: 26483036

35. Guo C, Khengar RH, Sun M, Wang Z, Fan A, Zhao Y. Acid-responsive polymeric nanocarriers for topical adapalene delivery. Pharm Res. 2014; 31(11):3051–9. https://doi.org/10.1007/s11095-014-1398-z PMID: 24805280

36. Almeida MA, Nadal JM, Grassiolli S, Paludo KS, Zawadzki SF, Cruz L, et al. Enhanced gastric tolerability and improved anti-obesity effect of capsaicinoids-loaded PCL microparticles. Mater Sci Eng C. 2014; 40:345–56.

37. Persenaire O, Alexandre M, Degée P, Dubois P. Mechanisms and kinetics of thermal degradation of poly (ε-caprolactone). Biomacromolecules. 2001; 2(1):288–94. PMID: 11749185

38. Bhakay A, Rahman M, Dave R, Bilgili E. Bioavailability Enhancement of Poorly Water-Soluble Drugs via Nanocomposites: Formulation–Processing Aspects and Challenges. Pharmaceutics. 2018; 10 (3):86.

39. Haq A, Dorrani M, Goodyear B, Joshi V, Michniak-Kohn B. Membrane properties for permeability testing: Skin versus synthetic membranes. Int J Pharm. 2018; 539(1–2):58–64. https://doi.org/10.1016/j.ijpharm.2018.01.029 PMID: 29366943

40. Zhao S, Wang Z, Wei X, Zhao B, Wang J, Yang S, et al. Performance improvement of polysulfone ultrafiltration membrane using PANiEB as both pore forming agent and hydrophilic modifier. J Memb Sci. 2011; 385:251–62.

41. Tolba MM, El-Gamal RM. Determination of adapalene in gel formulation by conventional and derivative synchronous fluorimetric approaches. Application to stability studies and in vitro diffusion test. Chem Cent J. 2016; 10(1):33.

42. Milanese A, Gorincioi E, Rajabi M, Vistoli G, Santaniello E. New synthesis of 6 [3-(1-adamantyl)-4-methoxyphenyl]-2-naphthoic acid and evaluation of the influence of adamantyl group on the DNA binding of a naphthoic retinoid. Bioorg Chem. 2011; 39(4):151–8. https://doi.org/10.1016/j.bioorg.2011.07.003 PMID: 21864882